AIMS Mathematics, 10(10): 24153–24178.
DOI: 10.3934/math.20251071
Received: 31 July 2025
Revised: 15 September 2025
Accepted: 25 September 2025
Published: 22 October 2025

https://www.aimspress.com/journal/Math

Research article

Mix-GENEO: A flexible filtration for multiparameter persistent homology detects digital images

Jiaxing He[1], Bingzhe Hou[1,*], Tieru Wu[1,2,*] and Yue Xin[3]

[1] School of Mathematics, Jilin University, Changchun, 130012, China
[2] School of Artificial Intelligence, Jilin University, Changchun, 130012, China
[3] School of Mathematical Science, Heilongjiang University, Harbin, 150080, China

* **Correspondence:** Email: houbz@jlu.edu.cn, wutr@jlu.edu.cn.

Abstract: Two important tasks in the field of topological data analysis (TDA) are building practical filtrations on objects and using TDA to detect the geometry and primarily topological structures. Motivated by these tasks, we have defined the difference between the two group equivariant non-expansive operators (GENEOs) by DGENEO and built multiparameter filtrations by operators on images named the multi-GENEO, multi-DGENEO, and mix-GENEO, and we proved the stability of both the interleaving distance and multiparameter persistence landscape of the multi-GENEO with respect to the pseudometric on images, modeled as bounded functions. We also gave an upper bound for the multi-DGENEO and mix-GENEO. In practical applications, we regarded the space of images on a discrete domain, and then we built multifiltrations on the discrete function space. Finally, we conducted a comparable experiment on the MNIST dataset to demonstrate that our bifiltrations are superior to 1-parameter filtrations. The experiment results demonstrate that our bifiltrations have the ability to detect geometric and topological differences of digital images.

Keywords: topological data analysis; multifiltration; interleaving distance; multiparameter persistence landscape; GENEOs
Mathematics Subject Classification: 55N31, 68T09

1. Introduction

The construction of filtration on images has always been an important issue in topological and geometric data analysis (TGDA). Currently, the sublevel set filtration to generate 1-parameter persistent homology is widely used. In Figure 1, we can see the lower-star filtration built on digit 3 from the MNIST dataset by [42] only generated H_0 barcode $(0, +\infty]$ and H_1 barcode $(0, 255]$, which are two meaningless signatures. We generate the persistence diagram by the Persim library [48]. For a given

filtration and a homological dimension p, the p-persistence diagram is given in the form of a multiset $D = \{(b_i, d_i) \in \mathbb{R}^2 | i \in I, b_i < d_i\}$, where each point $(b_i, d_i \in \mathbb{R}^2)$ corresponds to a topological feature born at scale b_i and dying at scale d_i. The diagram also includes the diagonal $y = x$, where each point on the diagonal is considered with infinite multiplicity. In [6], the authors defined group equivariant non-expansive operators (GENEOs), and in [51], the authors computed persistent homology on images by utilizing convolution operators. Compared to traditional sublevel set filtrations, their methods can improve accuracy to some extent, but our filtration can significantly enhance accuracy. By applying specific operators to images, H_1 persistent homology obtained from the 1-parameter sublevel set filtration can identify the digits 1 and 3. However, this filtration cannot significantly identify the digits 1 and 3, 6 and 9 in the MNIST dataset by H_1 persistent homology and GENEOs have never been used in combination with multiparameter persistent homology (MPH) in any context, not only on images. The multi-parameter filtrations on images are still in absence [20, 39, 54]. In this context, we propose three types of multifiltrations named the multi-GENEO, multi-DGENEO, and mix-GENEO. We conduct experiments to show the superior performance of multiparameter filtrations in MNIST digit recognition.

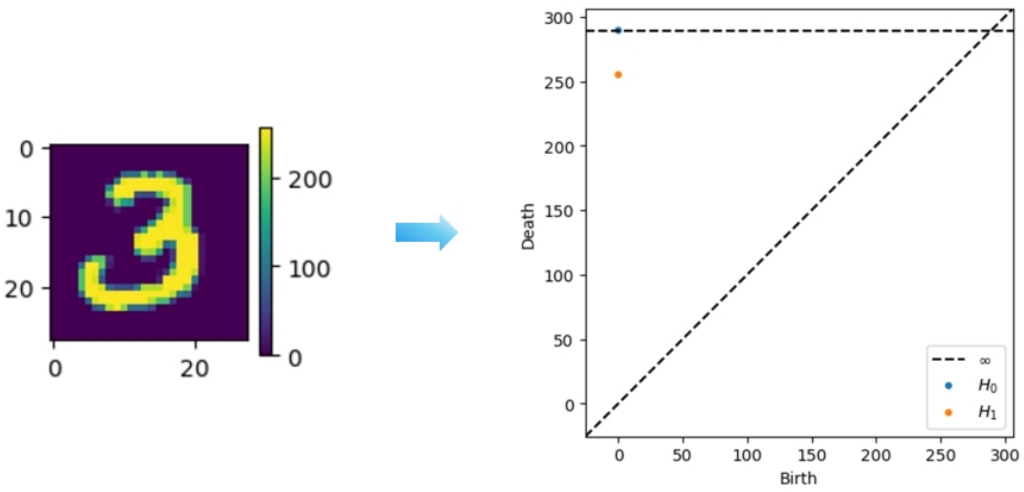

Figure 1. Persistence diagrams H_0 and H_1 generated by lower-star filtration on the digit 3. The orange point $(0, 255)$ in the persistence diagram represents the 1-dimensional loop appearing at 0 and disappearing at 255. The blue point $(0, +\infty)$ represents the connected component appearing at 0 and never disappearing.

In Figure 2, we show the barcodes associated with the persistence modules H_0 and H_1 obtained by generating the mix-GENEO filtration on the digit 3. The multiparameter persistence modules H_0 and H_1 provide more information about the shapes of the images.

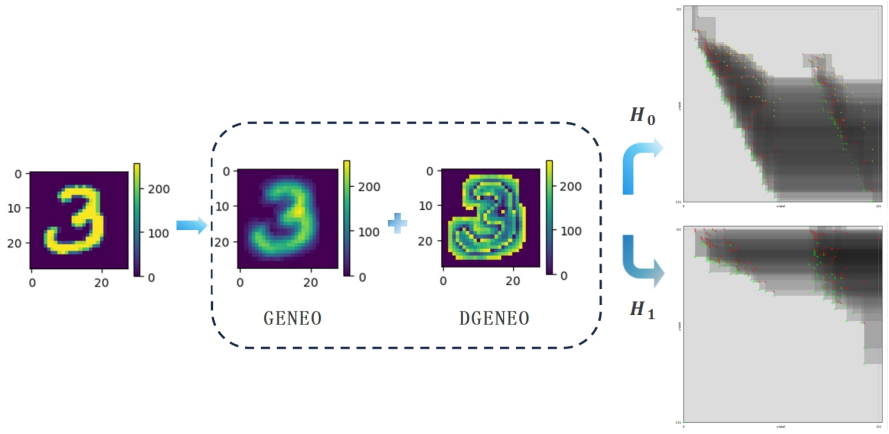

Figure 2. Multiparameter persistence modules H_0 and H_1 generated by mix-GENEO filtration on the digit 3.

1.1. Overview

Topological and geometric data analysis (TGDA) describes an emerging method to distinguish topological and geometric features combined with data analysis tools. While the history of TDA (topological data analysis) could date back to the 1990s, the field has been developed rapidly in recent years, which leads to rich theoretical foundations such as pseudo-metrics [9, 37] and persistence modules [5, 26], high efficient algorithms [23] and software [41, 42, 52], and a broad range of applications including medicine [46], optimization [35], deep learning [13, 36, 40], and manifold learning [33].

A ubiquitous tool in TGDA is persistence homology (PH). The theory of PH studies the homological group of a family of topological spaces and its representation, which is called the persistence module, see [43, 45] for details. In probability theory, several authors have proposed estimators of fractal dimension defined in terms of minimum spanning trees and higher dimensional persistent homology [1, 49, 50].

However, a single filtered space cannot often adequately capture the structure of interest in the data. This leads one to consider multiparameter persistence. Multiparameter persistence homology (MPH) was first considered in [19], in which they studied a multifiltration: A family of spaces parametrized along multiple dimensions. The algebraic invariants of these multifiltrations are called multiparameter persistence modules. Unlike the single persistence, there is no analogous complete discrete invariant for the multiparameter module.

In [14] and [53], the authors introduced the stable vectorization of the complete invariant of single parameter persistent homology, called the persistence landscape, and the stable vectorization of the multiparameter persistence module, called the multiparameter persistence landscape, respectively. Besides, another stable vectorization of the persistence diagram is the persistence image [2], which has been shown to produce favorable classification results when combined with machine learning methods. The multiparameter persistence image was introduced in [20], which is suitable for machine learning and statistical frameworks.

Moreover, by using the geometric features of data extracted by PH and MPH as inputs for statistic techniques, one can provide new insights into the data. A persistence diagram could mark the parameter

values for births and deaths of homological features. In a popular point of view, it is said that the long intervals represent the topological signal and the short intervals represent the noise. However, the authors [15] proved that persistent homology detects the curvature of disks, which shows that the short intervals also encode geometric information. From [3], persistent homology is a mathematically motivated out-of-the-box tool that one can use to summarize not only the global topology but also the local geometry of a wide variety of datasets.

Within the framework of 1-parameter persistent homology, there have been many proposals to build filtrations, including the removal of low density outliers [17], filtering by density functions and kernel density functions [11, 21, 44], measuring constructions by distances [4, 16, 32], and subsampling [8]. However, there are several disadvantages for 1-parameter persistence. For instance, 1-parameter persistence is only determined by one single parameter, and it can detect both small and large features. One of its main limitation is that it is insufficient to extract an adequate number of features.

Several methods to construct multiparameter filtrations for points have been proposed such as the superlevel-rips bifiltration [19], the multicover bifiltration [25] and the rhomboid bifiltration [28]. These approaches can be found in [10] for more details. In [20], the authors constructed a 2-parameter sublevelset filtration from a pair of two images from a piece of human tissue of a patient suffering from breast cancer.

1.2. Motivation

Many applications of 1-parameter persistent homology concern image analysis, where sublevel filtrations are often used. There is not yet a consensus on what the most natural or useful multifiltrations are for image analysis, but one promising idea is that a second persistence parameter can be used to thicken sublevel or superlevel sets, thereby introducing some sensitivity to the width of features that the ordinary sublevel and superlevel filtrations lack. One construction [22] along these lines is a framework that uses morphological operations to naturally form a multiparameter filtration to denoise.

We would like to build a multifiltration of digital images to compute multiparameter homology, and then detect significant topological and geometric features from the multiparameter persistent landscape.

The multiparameter landscape functions are sensitive to homological features of large, medium, and small persistence. The landscapes also have the advantage of being interpretable since they are closely related to the rank invariant [19].

Frequently in topological data analysis, we need to consider several $\mathbb{R}$-valued functions

$$\gamma_i : X \to \mathbb{R},\ i = 1, ..., n.$$

For $\boldsymbol{a} = (a_1, \cdots, a_n)$ and $\boldsymbol{b} = (b_1, \cdots, b_n)$, if $a_i \leq_n b_i$ for $i = 1, \cdots, n$, we say $\boldsymbol{a} \leq_n \boldsymbol{b}$. It is equivalent to consider a function $\gamma : X \to \mathbb{R}^n$ on a topological space X which gives rise to an n-parameter sublevelset filtration $\mathcal{S}(\gamma)$, defined by

$$\mathcal{S}(\gamma)_{\boldsymbol{s}} = \{\ y \in X \ \mid\ \gamma(y) \leq_n \boldsymbol{s},\ \boldsymbol{s} \in \mathbb{R}^n\ \}.$$

We want to explore the impact of different levels of filtration on the multiparameter persistence module. In [6], the authors defined group equivariant non-expansive operators (GENEOs) whose space is compact and convex with respect to the proper pseudometrics. Based on the stability, they described a simple strategy to select and sample operators and show how the operators can be used to perform machine learning. Also, they provided a flexible way to select operators. Since the GENEO can be

viewed as a form of Gaussian blur, and the Laplacian operator (often regarded as a sharpening tool) can be approximated by the subtraction of two Gaussian blurs of different scales (a method known as the Laplacian of Gaussian, or LOG), we denote the difference between two GENEOs by DGENEO, and we also call it DOG, for short. We can use GENEOs and DGENEOs to construct n-parameter persistent filtrations, which are named the multi-GENEO, multi-DGENEO, and mix-GENEO in the present paper.

To construct n-parameter filtrations from a data set, we represent data as functions. The following notations are from [6]. Suppose that X is a non-empty set and Φ is a topological subspace of the space of all bounded functions from X to $\mathbb{R}$. Obviously, Φ is naturally endowed with the topology induced by the distance $D_\Phi := \|\varphi_1 - \varphi_2\|_\infty$.

Denote by $Homeo(X)$ the set of all homeomorphisms from X to X. For $g \in Homeo(X)$, if for every $\varphi \in \Phi$, $\varphi \circ g \in \Phi$ and $\varphi \circ g^{-1} \in \Phi$, then we say g is a Φ-preserving homeomorphism. Denote by $Homeo_\Phi(X)$ the set of all $\Phi-$preserving homeomorphisms on X. Let G be a subgroup of $Homeo_\Phi(X)$, and the pair (Φ, G) is called a perception pair. Let (Φ, G), (Ψ, H) be two perception pairs and $T : G \to H$ be a fixed homomorphism. A fixed operator $F : \Phi \to \Psi$ is said to be a group equivariant operator from (Φ, G) to (Ψ, H) if $F(\varphi \circ g) = F(\varphi) \circ T(g)$ for every $\varphi \in \Phi$ and $g \in G$. Moreover, the definition of the GENEO is as follows:

Definition 1.1. *[6] Assume that (Φ, G), (Ψ, H) are two perception pairs and a homomorphism $T : G \to H$ has been fixed. If F is a group equivariant operator from (Φ, G) to (Ψ, H) with respect to T and F is non-expansive (i.e., $D_\Psi(F(\varphi_1), F(\varphi_2)) \leq D_\Phi(\varphi_1, \varphi_2)$ for every $\varphi_1, \varphi_2 \in \Phi$), then F is called a group equivariant non-expansive operator (GENEO) associated with $T : G \to H$.*

In this paper, we define the multi-GENEO, multi-DGENEO, and mix-GENEO as follows.

Definition 1.2. *A multi-GENEO filtration $\{\gamma_i\}_{i=1}^n$ is a multiparameter filtration defined by $\gamma_i = F^i(\varphi)$, where $\varphi \in \Phi$, and each F^i is a GENEO, $i = 1, ..., n$. A multi-DGENEO $\{\gamma_i\}_{i=1}^n$ is a multiparameter filtration defined by $\gamma_i = L^i(\varphi) = F^{1,i}(\varphi) - F^{2,i}(\varphi)$ where $\varphi \in \Phi$, and $F^{1,i}$ and $F^{2,i}$ are two elements in the space of GENEOs, $i = 1, ..., n$. Moreover, if each $\gamma_i = M^i$ is chosen to be $F^i(\varphi)$ or $L^i(\varphi)$ with at least one being $F^i(\varphi)$, we call $\{M^i\}_{i=1}^n$ a mix-GENEO and call M^i an MGENEO.*

The reason we select one component of MGENEOs as F^i is that we aim to utilize GENEOs to improve the accuracy of DGENEOs.

In [27], a filtration of K is a nested sequence of subcomplexes that starts with the empty complex and ends with the complete complex,

$$\emptyset = K_0 \subset K_1 \subset \cdots \subset K_m = K.$$

Remark 1.1. *Combining the above definition of filtration with a sublevelset filtration, multi-GENEO filtrations can yield multiparameter filtrations for digital images.*

1.3. Contributions

In this paper, we provide a flexible framework to build multiparameter filtrations on digital images.

• We define the DGENEO and introduce three methods to build multiparameter filtrations called the multi-GENEO, multi-DGENEO, and mix-GENEO.

• We show the stability of both interleaving distance and the multiparameter persistence landscape of multi-GENEOs, and also provide bound estimates for both multi-DGENEOs and mix-GENEOs with respect to the pseudometric for the subset of bounded functions.

• We conduct experiments on the MNIST dataset and demonstrate that our bifiltrations make sense in identifying features of persistence modules via machine learning methods, which shows the ability of the multiparameter persistent homology to detect geometric and topological differences in digital images.

• We compare the results of lower-star filtration, upper-star filtration, height filtration, radial filtration, density filtration, the multi-GENEO, the multi-DGENEO, and the mix-GENEO by ten-classification. The mix-GENEO performs the best.

To foster further developments at the intersection of multiparameter persistent homology and machine learning theory, we release our source code under: `https://github.com/HeJiaxing-hjx/Mix-GENEO/`.

2. Background

In this section, we will introduce some definitions and properties used in this paper.

Let $\mathbb{R}$ be the set of real numbers. For vectors $\boldsymbol{s}$, $\boldsymbol{t}$ in $\mathbb{R}^n$, there is a natural partial order on $\mathbb{R}^n$ by taking $(s_1, ..., s_n) \leq_n (t_1, ..., t_n)$ if and only if $s_i \leq t_i$ for all $1 \leq i \leq n$. Consider the sublevelset filtration

$$X_{\boldsymbol{s}} := \mathcal{S}(\gamma)_{\boldsymbol{s}} = \{\, y \in X \mid \gamma(y) \leq_n \boldsymbol{s} \,\}$$

with natural inclusion $\iota_{\boldsymbol{s},\boldsymbol{t}}$.

Denote by X the collection $\{X_{\boldsymbol{s}}\}_{\boldsymbol{s}\in\mathbb{R}^n}$ and denote by ι the collection of continuous maps $\iota_{\boldsymbol{s},\boldsymbol{t}} : X_{\boldsymbol{s}} \to X_{\boldsymbol{t}}$. Similarly, denote by Y a collection $\{Y_{\boldsymbol{s}}\}_{\boldsymbol{s}\in\mathbb{R}^n}$ and denote by $\tilde{\iota}$ the collection of inclusion maps $\tilde{\iota}_{\boldsymbol{s},\boldsymbol{t}} : Y_{\boldsymbol{s}} \to Y_{\boldsymbol{t}}$.

Denote by $\boldsymbol{Top}^{\mathbb{R}^n}$ the category whose objects are (X, ι) and whose morphisms are maps $f : (X, \iota) \to (Y, \tilde{\iota})$, which is a collection of all linear maps $\{f_{\boldsymbol{s}}\}$ for all $\boldsymbol{s} \in \mathbb{R}^n$ such that $f_{\boldsymbol{s}} : X_{\boldsymbol{s}} \to Y_{\boldsymbol{s}}$ and the diagram commutes.

$$\begin{array}{ccc} X_{\boldsymbol{s}} & \xrightarrow{\iota_{\boldsymbol{s},\boldsymbol{t}}} & X_{\boldsymbol{t}} \\ \downarrow{\scriptstyle f_{\boldsymbol{s}}} & & \downarrow{\scriptstyle f_{\boldsymbol{t}}} \\ Y_{\boldsymbol{s}} & \xrightarrow{\tilde{\iota}_{\boldsymbol{s},\boldsymbol{t}}} & Y_{\boldsymbol{t}} \end{array}$$

Now we will introduce the concept of a persistence module. Let $M = \oplus_{\boldsymbol{s}\in\mathbb{R}^n} M_{\boldsymbol{s}}$, where $M_{\boldsymbol{s}} = H_*(X_{\boldsymbol{s}})$ is a module. For any $\boldsymbol{s} \leq_n \boldsymbol{t}$, define the homomorphism $\tau_{\boldsymbol{s},\boldsymbol{t}} : M_{\boldsymbol{s}} \to M_{\boldsymbol{t}}$ by $\tau_{\boldsymbol{s},\boldsymbol{t}} = (\iota_{\boldsymbol{s},\boldsymbol{t}})_*(H_*(X_{\boldsymbol{s}}), H_*(X_{\boldsymbol{t}}))$, and then the following diagram commutes:

$$\begin{array}{ccc} M_{\boldsymbol{s}} & \xrightarrow{\tau_{\boldsymbol{s},\boldsymbol{t}}} & M_{\boldsymbol{t}} \\ & \searrow^{\tau_{\boldsymbol{s},\boldsymbol{r}}} & \downarrow{\scriptstyle \tau_{\boldsymbol{t},\boldsymbol{r}}} \\ & & M_{\boldsymbol{r}} \end{array}$$

when $\boldsymbol{s} \leq_n \boldsymbol{t} \leq_n \boldsymbol{r}$.

Denote by τ the collection of $\{\tau_{s,t}\}$ for all $\boldsymbol{s} \leq_n \boldsymbol{t}$. Denote by $M^{\mathbb{R}^n}$ the category whose objects are (M, τ) and whose morphisms are maps $h : (M, \tau) \to (N, \tilde{\tau})$, which is a collection of all continuous maps $\{h_s\}$ for all $\boldsymbol{s} \in \mathbb{R}^n$ such that $h_s : M_s \to N_s$ and the diagram commutes.

$$\begin{array}{ccc} M_{\boldsymbol{s}} & \xrightarrow{\tau_{s,t}} & M_{\boldsymbol{t}} \\ \downarrow{\scriptstyle h_s} & & \downarrow{\scriptstyle h_t} \\ N_{\boldsymbol{s}} & \xrightarrow{\tilde{\tau}_{s,t}} & N_{\boldsymbol{t}} \end{array}$$

Here (M, τ) and $(N, \tilde{\tau})$ are also called n-modules. For convenience, we use the notation M to represent the persistence module (M, τ).

To see more details about homology theory, we refer to [34].

Next, we would like to introduce three pseudometrics d_∞, d_I, and $d_\lambda^{(p)}$. Recall that an extended pseudometric on X is a function $d : X \times X \to [0, \infty]$ with the following three properties:

(1) $d(x, x) = 0$, for all $x \in X$.

(2) $d(x, y) = d(y, x)$, for all $x, y \in X$.

(3) $d(x, z) \leq d(x, y) + d(y, z)$, for all $x, y, z \in X$ with $d(x, y), d(y, z) < \infty$.

An extended metric is an extended pseudometric d with the additional property that $d(x, y) \neq 0$ whenever $x \neq y$. In this paper, we refer to extended (pseudo)metrics simply as (pseudo)metrics.

The filtrations of the multi-GENEO we constructed are sublevelset filtrations. For the topological space X, let $\gamma^X : X \to \mathbb{R}^n$ be a sublevelset filtration function. We can define an n-parameter sublevelset filtration $S(\gamma)$ of any function γ^X.

For a function $\gamma : X \to \mathbb{R}^n$, let

$$\|\gamma\| = \begin{cases} \sup_{p \in X} \|\gamma(p)\|_\infty & \text{if } X \neq \emptyset, \\ 0 & \text{if } X = \emptyset. \end{cases}$$

We are given $\gamma^X : X \to \mathbb{R}^n$ and $\gamma^Y : Y \to \mathbb{R}^n$ where Y is also a topological space. Let

$$d_\infty(\gamma^X, \gamma^Y) = \inf_{h \in \mathcal{H}} \|\gamma^X - \gamma^Y \circ h\|_\infty,$$

where $\mathcal{H}$ is the set of homeomorphisms from X to Y.

For $i \geq 0$, we say that a pseudometric d is i-stable for any topological spaces X, Y and any functions $\gamma^X : X \to \mathbb{R}^n$, $\gamma^Y : Y \to \mathbb{R}^n$. We have

$$d(H_i(\gamma^X), H_i(\gamma^Y)) \leq d_\infty(\gamma^X, \gamma^Y).$$

Moreover, we say a pseudometric is stable if it is i-stable if for all $i \geq 0$.

For $\epsilon \in \mathbb{R}$, let $\vec{\boldsymbol{\epsilon}} \in \mathbb{R}^n$ denote the vector whose components are each ϵ. Write $(\cdot)(\vec{\boldsymbol{\epsilon}}) : M^{\mathbb{R}^n} \to M^{\mathbb{R}^n}$ simply as $(\cdot)(\epsilon)$. Define $\tau_M^\epsilon : M_{\boldsymbol{a}} \to M_{\boldsymbol{a}+\vec{\boldsymbol{\epsilon}}}$ to be the morphism whose restriction to $M_{\boldsymbol{a}}$ is the linear map $\tau_{\boldsymbol{a},\boldsymbol{a}+\boldsymbol{\epsilon}}$. Simply write $M(\epsilon) = M_{\boldsymbol{a}+\vec{\boldsymbol{\epsilon}}}$. Two n-modules M and N are said to be ϵ-interleaved if there exist morphisms $f : M \to N(\epsilon)$ and $g : N \to M(\epsilon)$ such that

$$g(\epsilon) \circ f = \tau_M^{2\epsilon}, \ f(\epsilon) \circ g = \tau_N^{2\epsilon}.$$

Here, we call f and g ϵ-interleaving morphisms.

Define the interleaving distance $d_I : M \times N \to [0, \infty)$ as follows:

$$d_I(M, N) = \inf\{\epsilon \in [0, \infty) \mid M \text{ and } N \text{ are } \epsilon - \text{interleaved}\}.$$

The above d_I is the same as the definition in [37], and the stability of d_I is also given in [37].

Theorem 2.1. *[37] d_I is stable.*

The multiparameter persistence landscape proposed in [53] is a stable representation with respect to the interleaving distance and persistence weighted Wasserstein distance. The author also provided examples and statistical tests to demonstrate a range of potential applications which are convenient to utilize.

Let $M \in M^{\mathbb{R}^n}$. Consider the function $\lambda : \mathbb{N} \times \mathbb{R}^n \to \mathbb{R}$,

$$\lambda(k, \boldsymbol{x}) = \sup\{\varepsilon \geq 0 : \beta^{\boldsymbol{x}-\boldsymbol{h}, \boldsymbol{x}+\boldsymbol{h}} \geq k \text{ for all } \boldsymbol{h} \geq \boldsymbol{0} \text{ with } \|\boldsymbol{h}\|_\infty \leq \epsilon\},$$

where $\beta^{\boldsymbol{a},\boldsymbol{b}} = \dim(\mathrm{Im}(M_a \to M_b))$ is considered as the corresponding Betti number for $\boldsymbol{a} \leq \boldsymbol{b}$. The multiparameter persistence landscape of M is the set of such function $\lambda(k, \boldsymbol{x})$ that describes the maximal radius over which k features persist in every (positive) direction through $\boldsymbol{x}$ in the parameter space.

Let M, N be multiparameter persistence modules. The *p-landscape* distance $d_\lambda^{(p)}(M, N)$ between M and N is defined by

$$d_\lambda^{(p)}(M, N) = \|\lambda(M) - \lambda(N)\|_p,$$

where $\|\cdot\|$ is the *L^p-norm* for the $\mathbb{R}$-valued functions on $\mathbb{N} \times \mathbb{R}^n$.

Theorem 2.2. *[53] Let $M, N \in M^{\mathbb{R}^n}$ be multiparameter persistence modules, and then the ∞ − landscape distance of the multiparameter persistence landscapes is bounded by the interleaving distance d_I, i.e.,*

$$d_\lambda^{(\infty)}(M, N) \leq d_I(M, N).$$

In [29,30], the authors considered the invariance of the persistent homology under homeomorphism actions.

Remark 2.1. *[30] It is easy to check that the persistent homology groups (and hence also the persistent Betti number functions) are invariant under the action of Homeo(X).*

We would like to introduce lower-star filtration and upper-star filtration, which are both 1-parameter filtrations. Let K be a triangulation of a compact 2-manifold without boundary $\mathbb{M}$. Let $h : \mathbb{M} \to \mathbb{R}$ be a function that is linear on every triangle. The function is defined, consequently, by its value at the vertices of K. We will assume that $h(u) \neq h(v)$ for all vertices $u \neq v \in K$. It is common to refer to h as the height function. In a simplicial complex, the natural concept of a neighborhood of a vertex u is the *star*, Stu, that consists of u together with the edges and triangles that share u as a vertex. Since all vertices have different heights, each edge and triangle has a unique lowest and a unique highest vertex. We can partition the simplicies of the star into lower and upper stars.

Definition 2.1. *[56] The lower star* $\underline{\mathrm{St}}u$ *and upper star* $\bar{\mathrm{St}}u$ *of vertex u for the height function h are*

$$\underline{\mathrm{St}}u = \{\sigma \in Stu \mid h(v) \leq h(u), \forall vertices\ v \in \sigma\}$$

and

$$\bar{\mathrm{St}}u = \{\sigma \in Stu \mid h(v) \geq h(u), \forall vertices\ v \in \sigma\}.$$

These subsets of the star contain the simplices that have u as their highest or their lowest vertex, respectively (by the usual definition, the star of u is the set of all simplices containing u and all of their faces). Let K be the union of either lower or upper stars, $K = \cup_u \underline{\mathrm{St}}u = \cup_u \bar{\mathrm{St}}u$. Then we can get a filtration. Suppose we sort the n vertices of K in order of increasing height to get the sequence u^1, u^2, ..., u^n, $h(u^i) < h(u^j)$, for all $1 \leq i < j \leq n$. We then let K^i be the union of the first i lower stars, $K^i = \cup_{1 \leq j \leq i} \underline{\mathrm{St}}u^j$. Each simplex σ has an associated vertex u^i, and we call the height of that vertex the birth time $h(\sigma) = h(u^i)$ of σ. The subcomplex K^i of K consists of the i lowest vertices together with all edges and triangles connecting them. Clearly, the sequence K^i defines a filtration of K. We may define another filtration by sorting in decreasing order and using upper stars.

We also give the definitions of height filtration, radial filtration, and density filtrations. For more details, we refer to [24, 31]. Let $\mathcal{B} : \mathcal{I} \subseteq \mathbb{Z}^d \to \{0, 1\}$ be a binary image.

For cubical complexes, we construct a height filtration $\mathcal{H} : \mathcal{I} \to \mathbb{R}$ of a d-dimensional binary image $\mathcal{I}$ by choosing a direction $v \in \mathbb{R}^d$ of norm 1 and defining new values on all the voxels of value 1 as follows: if $p \in \mathcal{I}$ is such that $B(p) = 1$, then one assigns a new value $H(p) := \ < p, v >$, the distance of p to the hyperplane defined by v. If $B(p) = 0$, then $\mathcal{H}(p) := \mathcal{H}_\infty$, where $\mathcal{H}_\infty$ is the filtration value of the pixel that is the farthest away from the hyperplane.

The radial filtration of $\mathcal{R}$ of $\mathcal{I}$ with center $c \in \mathcal{I}$ is defined by assigning to a voxel p the value corresponding to its distance to the center:

$$\mathcal{R}(p) := \begin{cases} \|c - p\|_2 & \text{if } \mathcal{B}(p) = 1, \\ \mathcal{R}_\infty & \text{if } \mathcal{B}(p) = 0, \end{cases}$$

where $\mathcal{R}_\infty$ is the distance of the pixel that is the farthest away from the center.

The density filtration gives each pixel a value depending on the number of neighbors it has at a certain distance. For a parameter r, the density filtration is:

$$\mathcal{D}_e(p) := \#\{v \in \mathcal{I}, \mathcal{B}(v) = 1 \text{ and } \|p - v\| \leq r\},$$

where the norm can be any norm on $\mathbb{R}^d$, and we choose the $L1$-norm.

3. Stability and representation

In this section, we will show the stability and the bound estimates with respect to both the interleaving distance and multiparameter persistence landscape of the multi-GENEO, multi-DGENEO, and mix-GENEO persistence modules. We will also show the filtrations of the multi-GENEO, multi-DGENEO, and mix-GENEO on discrete function spaces.

3.1. Stability for the multi-GENEO

Consider F as an element in the direct sum of n copies of the GENEO written as $F = (F^1, F^2, ..., F^n) \in \bigoplus_{i=1}^n GENEO$.

Theorem 3.1. *Let X be a non-empty space, $\varphi_k \in \Phi$ be the bounded functions on X for $k = 1, 2$, and $\bigoplus_{I=1}^n$ GENEO be the space of multi-GENEOs. Endow the space of multi-GENEOs with the topology induced by the uniform norm. Then,*

$$\sup_{F \in \bigoplus_{I=1}^n \mathrm{GENEO}} d_\lambda^{(\infty)}(V(\mathcal{S}(F(\varphi_1))), V(\mathcal{S}(F(\varphi_2)))) \leq \|\varphi_1 - \varphi_2\|_\infty ,$$

where $V(\mathcal{S}(F(\cdot)))$ denotes the multiparameter persistence module of $\mathcal{S}(F)$.

Proof. Let G be a subgroup of $\mathrm{Homeo}_\Phi(X)$. For every $F \in \bigoplus_{i=1}^n GENEO$, every $g \in G$, and φ_1, $\varphi_2 \in \Phi$, we have that

$$\begin{aligned}
d_I(V(\mathcal{S}(F(\varphi_1))), V(\mathcal{S}(F(\varphi_2)))) &= d_I(V(\mathcal{S}(F^1(\varphi_1), ..., F^n(\varphi_1))), V(\mathcal{S}(F^1(\varphi_2), ..., F^n(\varphi_2))))\\
&= d_I(V(\mathcal{S}(F^1(\varphi_1), ..., F^n(\varphi_1))), V(\mathcal{S}(F^1(\varphi_2)\circ T(g), ..., F^n(\varphi_2)\circ T(g))))\\
&= d_I(V(\mathcal{S}(F^1(\varphi_1), ..., F^n(\varphi_1))), V(\mathcal{S}(F^1(\varphi_2\circ g), ..., F^n(\varphi_2\circ g))))\\
&\le D_\Psi((F^1(\varphi_1), ..., F^n(\varphi_1)), (F^1(\varphi_2\circ g), ..., F^n(\varphi_2\circ g))\\
&= \|(F^1(\varphi_1-\varphi_2\circ g), ..., F^n(\varphi_1-\varphi_2\circ g))\|_\infty\\
&= \max_i \|F^i(\varphi_1-\varphi_2\circ g)\|_\infty\\
&\le \|\varphi_1-\varphi_2\circ g\|_\infty\\
&= D_\Phi(\varphi_1, \varphi_2\circ g),
\end{aligned}$$

where D_Ψ is a distance defined by $D_\Psi(\psi_1, \psi_2) = \|\psi_1 - \psi_2\|_\infty$. The second equality follows from the invariance of multiparameter persistent homology under the action of $\mathrm{Homeo}_\Phi(X)$, which is easy to see by Remark 2.1. The third equality and the seventh inequality follow from that each F^i is a GENEO. The fourth inequality follows from the stability of multiparameter persistent homology while the sixth equality follows from the definition of the metric $\|\cdot\|_\infty$. Since φ_1, φ_2, g are arbitrarily chosen and F is an element in the direct sum of n copies of the GENEO, we get

$$\sup_F d_I(V(\mathcal{S}(F(\varphi_1))), V(\mathcal{S}(F(\varphi_2)))) \le \inf_{g\in G} \|\varphi_1-\varphi_2\circ g\|_\infty \le D_\Phi(\varphi_1, \varphi_2).$$

Furthermore, by Theorem 2.2, we have that

$$\begin{aligned}
\sup_F d_\lambda^{(\infty)}(V(\mathcal{S}(F(\varphi_1))), V(\mathcal{S}(F(\varphi_2)))) &\le \sup_F d_I(V(\mathcal{S}(F(\varphi_1))), V(\mathcal{S}(F(\varphi_2))))\\
&\le \inf_{g\in G} \|\varphi_1-\varphi_2\circ g\|_\infty\\
&\le D_\Phi(\varphi_1, \varphi_2).
\end{aligned}$$

The third inequality follows from the property that D_Φ is G-invariant.

Then we obtain the stability of the ∞-landscape distance of the multiparameter persistence landscapes. □

Consider $L = (L^1, L^2, \cdots, L^n)$. Let $L^i(\varphi) = F^{1,i}(\varphi) - F^{2,i}(\varphi)$, for which $F^{1,i}$ and $F^{2,i}$ are two elments in the GENEOs, $i = 1, ..., n$. Then we have $L \in \bigoplus_{I=1}^n \mathrm{DGENEO}$.

Lemma 3.1. *Let X be a non-empty space, $\varphi_k \in \Phi$ be the bounded functions on X for $k = 1, 2$, and $\bigoplus_{I=1}^n \mathrm{DGENEO}$ be the space of multi-DGENEOs. Endow the space of multi-DGENEOs with the topology induced by the uniform norm. Then*

$$\sup_{L\in\bigoplus_{I=1}^n \mathrm{DGENEO}} d_\lambda^{(\infty)}(V(\mathcal{S}(L(\varphi_1))), V(\mathcal{S}(L(\varphi_2)))) \le 2\|\varphi_1-\varphi_2\|_\infty.$$

Proof. The same as in the calculation in Theorem 3.1, let G be a subgroup of $Homeo_{\Phi}(X)$, and we have

$$\begin{aligned} d_I(V(\mathcal{S}(L(\varphi_1))), V(\mathcal{S}(L(\varphi_2)))) &\leq D_{\Psi}((L^1(\varphi_1), ..., L^n(\varphi_1)), (L^1(\varphi_2 \circ g), ..., L^n(\varphi_2 \circ g))) \\ &= \max_i \|L^i(\varphi_1 - \varphi_2 \circ g)\|_{\infty} \\ &\leq 2\|\varphi_1 - \varphi_2 \circ g\|_{\infty} \\ &= 2D_{\Phi}(\varphi_1, \varphi_2 \circ g). \end{aligned}$$

Since φ_1, φ_2, g are arbitrarily chosen and F is considered as an element in the direct sum of n copies of the GENEO, the conclusion is obtained. □

Consider $M = (M^1, M^2, \cdots, M^n)$, where M^i is either F^i or L^i with at least one being F^i. Then we have $M \in \bigoplus_{i=1}^n$ MGENEO. Since each $F^i \in$ GENEO can be written as $F^i - 0 \in$ DGENEO, we have $M \in \bigoplus_{i=1}^n$ DGENEO and MGENEO $\subseteq$ DGENEO.

Corollary 3.1. *Endow the space of mix-GENEOs with the topology induced by the uniform norm. Let $V(S(M(\varphi_k)))$ be the multiparameter persistence module of the mix-GENEO, $k = 1, 2$. Then*

$$\sup_M d_{\lambda}^{(\infty)}(V(\mathcal{S}(M(\varphi_1))), V(\mathcal{S}(M(\varphi_2)))) \leq 2\,\|\varphi_1 - \varphi_2\|_{\infty}\,.$$

Proof. The same as in the proof in Lemma 3.1, we can use Definition 1.2 to get the conclusion. □

The pipeline of Theorem 3.1, Lemma 3.1, and Corollary 3.1 is summarized in Figure 3.

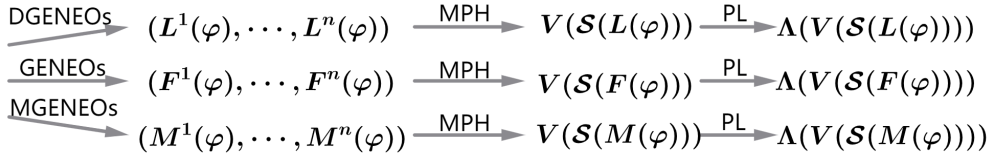

Figure 3. Pipline. $V(F(\varphi))$, $V(L(\varphi))$, and $V(M(\varphi))$ denote the multiparameter persistence module associated with $(F^1, F^2, ..., F^n)$, $(L^1, L^2, ..., L^n)$, and $(M^1, M^2, ..., M^n)$, respectively. Λ denotes their persistence landscape's vectorization.

3.2. Representation on discrete function spaces

Similar to the representation on discrete function spaces of 1-parameter GENEO construction in [6], we can construct filtrations of the multi-GENEO, multi-DGENEO, and mix-GENEO. For a positive integer k, let $\{\sigma_j\}_{j=1}^k$ be a sequence of positive numbers and $\{\tau_j\}_{j=1}^k$ be a sequence of real numbers. We consider that $\{g_{\tau_j}\}_{j=1}^k$ for each $g_{\tau_j} : \mathbb{R} \to \mathbb{R}$ is a 1-dimensional Gaussian function with width σ_j and center τ_j,

$$g_{\tau_j}(t) := \exp\left\{-\frac{(t-\tau_j)^2}{2(\sigma_j)^2}\right\}.$$

Let S be the set of $p_i = (a_1^i, \tau_1^i, ..., a_k^i, \tau_k^i) \in \mathbb{R}^{2k}$ satisfying that $\sum_{j=1}^k (a_j^i)^2 = \sum_{j=1}^k (\tau_j^i)^2$ and let $p = (p_1, \cdots, p_n)$, where $i = 1, \cdots, n$. Define the function $G_p = (G_{p_1}^1, ..., G_{p_n}^n)$ by

$$G_{p_i}^i(x, y) := \sum_{j=1}^k a_j^i g_{\tau_j^i}(\sqrt{x^2 + y^2}).$$

Define the convolutional operator $F^i_{p_i}$ as follows. For each continuous map $\varphi : \mathbb{R}^2 \to \mathbb{R}$ with compact support, $F^i_{p_i}(\varphi) : \mathbb{R}^2 \to \mathbb{R}$ is the continuous map with compact support in the following form:

$$F^i_{p_i}(\varphi)(x,y) := \int_{\mathbb{R}^2} \varphi(\alpha,\beta)\frac{G^i_{p_i}(x-\alpha, y-\beta)}{\|G^i_{p_i}\|_{L^1}} d\alpha d\beta.$$

Given $\Phi := \{\varphi\colon \mathbb{R}^2 \to \mathbb{R} \text{ with compact support}\}$, $\mathrm{Iso}(\mathbb{R}^2)$, the group of Euclidean plane isometries, and T, the identity homomorphism, then $F^i_{p_i}$ is a GENEO from $(\Phi, \mathrm{Iso}(\mathbb{R}^2))$ to itself. One can see that $\{F^i_{p_i}(\varphi)\}_{i=1}^n$ contributes to a filtration of the multi-GENEO. Then by Definition 1.2, $L^i(\varphi) = F^{1,i}_{p1_i}(\varphi) - F^{2,i}_{p2_i}(\varphi)$ for $i = 1, ..., n$, and we can also get the filtration of the multi-DGENEO and mix-GENEO.

Remark 3.1. *We will show that each $F^i_{p_i}$ is a GENEO. For each $h \in Iso(\mathbb{R}^2)$, we have $h(\alpha,\beta) = A(\alpha,\beta)^T + (b_1, b_2)^T$ for any $(\alpha,\beta) \in \mathbb{R}^2$, where A is an orthogonal matrix. Notice that for any $(\alpha,\beta), (x,y) \in \mathbb{R}^2$,*

$$\|h(x,y) - h(\alpha,\beta)\|_2 = \|(x,y) - (\alpha,\beta)\|_2,$$

where $\|(x,y)\|_2 = \sqrt{x^2+y^2}$. Then

$$G^i_{p_i}((x,y) - (\alpha,\beta)) = G^i_{p_i}(h(x,y) - h(\alpha,\beta)).$$

For convenience, write $(\widetilde{\alpha},\widetilde{\beta}) = h(\alpha,\beta)$. One can see that

$$\begin{aligned} F^i_{p_i}(\varphi \circ h)(x,y) &= \int_{\mathbb{R}^2} \varphi(h(\alpha,\beta))\frac{G^i_{p_i}(x-\alpha, y-\beta)}{\|G^i_{p_i}\|_{L^1}} d\alpha d\beta \\ &= \int_{\mathbb{R}^2} \varphi(\widetilde{\alpha},\widetilde{\beta})\frac{G^i_{p_i}((x,y) - h^{-1}(\widetilde{\alpha},\widetilde{\beta}))}{\|G^i_{p_i}\|_{L^1}} |A^{-1}| d\widetilde{\alpha} d\widetilde{\beta} \\ &= \int_{\mathbb{R}^2} \varphi(\widetilde{\alpha},\widetilde{\beta})\frac{G^i_{p_i}(h(x,y) - (\widetilde{\alpha},\widetilde{\beta}))}{\|G^i_{p_i}\|_{L^1}} d\widetilde{\alpha} d\widetilde{\beta} \\ &= F^i_{p_i}(\varphi)(h(x,y)). \end{aligned}$$

Then, we obtain that

$$F^i_{p_i}(\varphi \circ h) = F^i_{p_i}(\varphi) \circ T(h).$$

Next, we will show that $F^i_{p_i}$ is non-expansive. For any $(x,y) \in \mathbb{R}^2$,

$$\begin{aligned} |F^i_{p_i}(\varphi(x,y)) - F^i_{p_i}(\psi(x,y))| &= \left| \int_{\mathbb{R}^2} (\varphi(\alpha,\beta) - \psi(\alpha,\beta))\frac{G^i_{p_i}(x-\alpha, y-\beta)}{\|G^i_{p_i}\|_{L^1}} d\alpha d\beta \right| \\ &\le \sup_{(\alpha,\beta)\in\mathbb{R}^2} |\varphi(\alpha,\beta) - \psi(\alpha,\beta)| \cdot \int_{\mathbb{R}^2} \frac{|G^i_{p_i}(x-\alpha, y-\beta)|}{\|G^i_{p_i}\|_{L^1}} d\alpha d\beta \\ &\le \sup_{(\alpha,\beta)\in\mathbb{R}^2} |\varphi(\alpha,\beta) - \psi(\alpha,\beta)|. \end{aligned}$$

Therefore, we have $\|F^i_{p_i}(\varphi) - F^i_{p_i}(\psi)\|_\infty \le \|\varphi - \psi\|_\infty$.

4. Experiments

In this section, we aim to demonstrate the effectiveness of our method in previously analyzed scenarios. We will use the multi-GENEO, multi-DGENEO, and mix-GENEO to extract multiparameter filtration from the MNIST dataset, and we will use the tool RIVET and multiparameter persistence landscape to represent the rank invariants of the multiparameter persistence modules. To construct comparable experiments, we use Dionysus to build 1-parameter filtrations on images and use persistence landscapes to vectorize their persistence diagrams.

RIVET is used to provide the corresponding results in the biparameter persistence module. RIVET software can compute and visualize three such kinds of invariants, the Hilbert function, the bigraded Betti numbers, and the fibered barcode. RIVET supports the fast computation of multigraded Betti numbers and an interactive visualization for 2-parameter persistence modules. RIVET approximates multiparameter modules with a discretization in order to reduce computational cost. These approximations can be taken to arbitrary accuracy with respect to the interleaving distance. Details of the time and space complexity of the algorithm may be found in [38, 52, 55].

Multiparameter persistence landscapes are stable with respect to the interleaving distance and persistence weighted Wasserstein distance which can be found in `https://github.com/OliverVipond/Multiparameter_Persistence_Landscapes/`. [53] provided statistical tests to demonstrate their potential applications of landscapes.

Dionysus is written in C++, with Python bindings, which provides various algorithms with clean and consistent internal design for computing persistent homology, which can be founded in `https://mrzv.org/software/dionysus2/`. This package is useful to build lower-star and upper-star filtrations of the Freudenthal triangulation on a grid.

Persistence Landscape is a useful and stable vector representation of persistence diagrams, which is proposed in [14]. It provides an efficient and easily understandable approach to vectorize persistence diagrams for machine learning tasks. These experiments are performed on Python packages from `https://persim.scikit-tda.org/`.

All experiments were run on a laptop with an AMD Ryzen 7 5800H with Radeon graphics and 16GB of memory.

4.1. Generating bifiltrations on digital images

In this subsection, we will provide an algorithm to generate biparameter filtrations on digital images, which is also suitable for n-parameter filtrations. We give an example to show how to generate biparameter filtration on digital images.

There have been several methods to construct cubical complexes. The authors in [47] represented the voxels as vertices of the cubical complexes, and then the authors in [7] used this method to build cubical complexes from an image $\varphi : X \to \mathbb{R}$. In [42], the author built lower-star and upper-star filtrations of the Freudenthal triangulation on a grid in Dionysus. Inspired by their contributions, we build a simplicial complex from two images $\varphi_1, \varphi_2 \in \Phi$ by considering a unit square as two 2-simplices.

Recall that such a grayscale image is a function $\varphi : X \to \mathbb{R}$, where $X \subset \mathbb{Z}^2$ is typically a rectangular subset of the discrete lattice

$$X = \{(m, n) \mid 0 \leq m \leq M, 0 \leq n \leq N\}.$$

A point $x = (m, n) \in X$ is called a pixel and the value $\varphi(x) \in \mathbb{R}$ is called the grayscale value of x. The pixels in X are the vertices (0-cells) of the complex. If two vertices whose coordinates differ by one in a single axis, then the edge with endpoints of the two vertices is one 1-simplex. If four vertices form a unit square, then the edge with endpoints located in the upper left and the lower right is also one 1-simplex. And then, the unit square is divided into two 2-simplices. An example is given in Figure 4.

Figure 4. The solid dots represent vertices that have already appeared. There is one edge with two endpoints in the left figure and there are two 2-simplices colored in yellow.

Suppose that two grayscale digital images φ_1 and φ_2 are represented by the following two matrices:

$$\begin{bmatrix} 7 & 5 & 3 \\ 8 & 6 & 9 \\ 1 & 4 & 2 \end{bmatrix} \quad \text{and} \quad \begin{bmatrix} 3 & 2 & 7 \\ 4 & 9 & 8 \\ 5 & 6 & 1 \end{bmatrix}.$$

Then we use nine letters from a to i to mark the nine vertices as follows:

$$\begin{array}{ccc} \bullet & \bullet & \bullet \\ \bullet & \bullet & \bullet \\ \bullet & \bullet & \bullet \end{array} \qquad \begin{array}{ccc} g & h & i \\ d & e & f \\ a & b & c \end{array}$$

By taking sublevelset filtration, a bifiltration is shown in Figure 5. The classes in the position (p, q) are generated by the pixels x which satisfying $\varphi_1(x) \leq p$ and $\varphi_2(x) \leq q$. Notice that the 0-simplices in the position $(4, 6)$ are a, b, and c, and the 1-simplices are ab and bc. The simplices b, ab, and bc first appear in the position $(4, 6)$. Call (p, q) the birth coordinate of them.

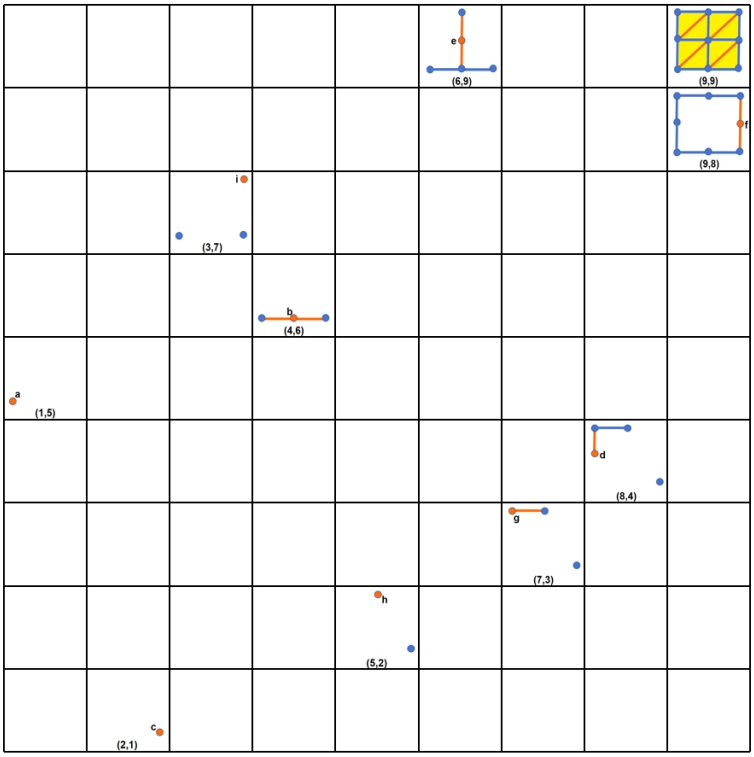

Figure 5. Bifiltration example. The figure records the birth coordinates of vertices, edges, and faces, and refers to the previously defined functions φ_1 and φ_2. The vertices and edges in the birth coordinates are colored in orange, the faces in the birth coordinates are colored in yellow, and the rest are colored in blue.

Furthermore, we can use RIVET to visualize the biparameter persistence modules of 0-dimensional and 1-dimensional homology in Figure 6. For details of basic persistent homology, please refer to [12, 55, 56].

$\mathscr{B}_{H(X)^0}$ $\mathscr{B}_{H(X)^1}$

Figure 6. $\mathscr{B}_{H(X)^0}$ reprensents the H_0 multiparameter persistence module and $\mathscr{B}_{H(X)^1}$ represents the H_1 multiparameter persistence module. One can see 1-loop in $\mathscr{B}_{H(X)^1}$, only birth at the coordinate (9,8), and persist to the coordinate (9,9).

Notice that the bifiltration is a one-critical multifiltration defined in [18] since each cell of the multifilter complex has a unique critical coordinate.

Algorithm 1 Build bifiltration.

Input: $\mathcal{V}$, vertex;
Input: φ, image;
Input: $M = (M^1, M^2)$, mix-GENEO (or multi-GENEO, or multi-DGENEO);
Output: $\mathscr{F} = (\mathscr{F}_x, \mathscr{F}_y)$, bifiltration at (x, y);

$\psi_1 = M^1(\varphi)$, $\psi_2 = M^2(\varphi)$;
$\mathscr{F}$ ←empty;
for $v \in \mathcal{V}$ **do**;
$(\mathscr{F}_{vx}, \mathscr{F}_{vy}) = (\psi_1(v), \psi_2(v))$;
$\mathscr{F} \leftarrow \mathscr{F} \bigcup (\mathscr{F}_{vx}, \mathscr{F}_{vy})$;
end for
$\mathcal{E}$ ←empty;
if v_i is adjacent to v_j **then**
$\mathcal{E} \leftarrow \mathcal{E} \bigcup \{e_{ij}\}$;
end if
for $e_{ij} \in \mathcal{E}$ **do**;
$(\mathscr{F}_{e_{ij}x}, \mathscr{F}_{e_{ij}y})$
$= (\max(\mathscr{F}_{v_ix}, \mathscr{F}_{v_jx}), \max(\mathscr{F}_{v_iy}, \mathscr{F}_{v_jy}))$;
$\mathscr{F} \leftarrow \mathscr{F} \bigcup (\mathscr{F}_{e_{ij}x}, \mathscr{F}_{e_{ij}y})$;
end for
$\mathcal{F}$ ←empty;
if four vertices v_i, v_j, v_k, v_s form a square, and e_{ik} is a diagonal line in the square with a fixed direction; **then**
$\mathcal{F} \leftarrow \mathcal{F} \bigcup f_{ijk}$;
$\mathcal{F} \leftarrow \mathcal{F} \bigcup f_{isk}$;
end if
for $f_{ijk}, f_{isk} \in \mathcal{F}$ **do**;
$(\mathscr{F}_{f_{ijk}x}, \mathscr{F}_{f_{ijk}y})$
$= (\max(\mathscr{F}_{v_ix}, \mathscr{F}_{v_jx}, \mathscr{F}_{v_kx}, \mathscr{F}_{v_sx}),$
$\max(\mathscr{F}_{v_iy}, \mathscr{F}_{v_jy}, \mathscr{F}_{v_ky}, \mathscr{F}_{v_sy}))$;
$(\mathscr{F}_{f_{isk}x}, \mathscr{F}_{f_{isk}y})$
$= (\max(\mathscr{F}_{v_ix}, \mathscr{F}_{v_jx}, \mathscr{F}_{v_kx}, \mathscr{F}_{v_sx}),$
$\max(\mathscr{F}_{v_iy}, \mathscr{F}_{v_jy}, \mathscr{F}_{v_ky}, \mathscr{F}_{v_sy}))$;
$\mathscr{F} \leftarrow \mathscr{F} \bigcup (\mathscr{F}_{f_{ijk}x}, \mathscr{F}_{f_{ijk}y}) \bigcup (\mathscr{F}_{f_{isk}x}, \mathscr{F}_{f_{isk}y})$;
end for
return $\mathscr{F}$.

Complexity. We now explore the complexity of Algorithm 1. Notice that the bifiltration we construct is all one-critical. One vertex is computed one time if it is a 0-simplex or a vertex of a higher simplex. A vertex is a common vertex of at most six 1-simplices and six 2-simplices. The algorithm requires at most $O(13n)$ time for n vertices. The running time for generating a bifiltration on a set of 100 images (each of size 28×28) is approximately 2.77 seconds.

4.2. Example computations

In this subsection, we will provide examples of computing binary classification and ten-classification. We compare the performance of 1-parameter filtrations (lower-star filtration, upper-star filtration, height filtration, radial filtration, and density filtration) with our multi-GENEO, multi-DGENEO, and mix-GENEO filtrations in the classification tasks by vectorizations. All the filtrations to be compared are built using the MNIST dataset.

Suppose that a digital image is a bounded function φ. We select five GENEOs, G_0, G_1, G_2, G_3, and G_4, to get bifiltration $\{F_p^i(\varphi)\}_{i=1}^2$. Previously, the notation G denoted a convolution kernel, while F was used for the GENEO associated with the convolution G and the input function φ. Notice that G_0 can be seen as a Gaussian blur, $G_2 - G_1$ and $G_4 - G_3$, which are called DOG, can be seen as Laplace operators approximately. Since Id is also a GENEO, we build multi-GENEO filtration by G_0 and Id acting on φ via right composition. Multi-DGENEO fitration is built by $\varphi \circ (G_4 - G_3)$ and $\varphi \circ (G_2 - G_1)$, and mix-GENEO filtration is built by $\varphi \circ G_0$ and $\varphi \circ (G_4 - G_3)$. To provide global information about the number of connected components as well as their positions in the image such as 6 and 9, the GENEOs we take are not composed of rotations (see the Appendix for the specific G_0, G_1, G_2, G_3, and G_4 we use). To make the parameters in RIVET and the persistence landscape consistent, we resize the value of $F_p^i(\varphi)$ into $[0, 255]$.

1-parameter filtrations. We use Dionysus to build 1-parameter filtrations. For the barcode generated by upper-star filtration, the birth time is later than the death time, so we swapped the birth time and death time of the barcodes generated by upper filtration. For the height filtration, radial filtration, and density filtration, we binarize the image according to a pixel value threshold of 40% as was done in [24, 31]. We set the vector $v = (1, 0)$ for height filtration and the center $c = (0, 0)$ for radial filtration. For 1-parameter filtrations, we set the stepsize of the persistence landscape $s = 10$, and set the parameter range to be $(0, \max)$, where max is the highest pixel-value of the corresponding dataset. 1-parameter filtrations are vectorized by the persistence landscape [14].

2-parameter filtrations. For 2-parameter filtrations, we use RIVET to build our three multifiltrations. To make the operation faster, we use the parameter bin in RIVET equal to 10 which coarsens the persistence module to obtain an algebraically simpler module. For 2-parameter filtrations, we set the persistence landscape $\lambda(k, \boldsymbol{x})$ for $k = 1$ in the parameter range $[0, 255]^2$ of the MNIST dataset with stepsize $s = 10$ for the H_0-modules and H_1-modules. Here the first landscape $\lambda(k, \boldsymbol{x})$ detects the parameter values for which the associated space has at least 1-homological features together with the persistence of those features. 2-parameter filtrations are vectorized by multiparameter persistence landscapes [53].

Machine learning classifiers. We use machine learning algorithms with persistence landscape and multiparameter landscape functions as a collection of features for a dataset to learn nonlinear relationships in our dataset. We use three machine learning classifiers: support vector machine (SVM) with an RBF kernel, convolutional neural network (CNN), and random forest (RF) with 100 trees. Before conducting SVM classification, we first use principal component analysis (PCA) to reduce the dimensionality of the features. We train a three-layer convolutional neural network using single-channel inputs for H_0 and H_1, respectively, and dual-channel inputs for $H_0 + H_1$.

Dataset. The MNIST dataset is a classic dataset in the field of machine learning, consisting of 60,000 training samples and 10,000 test samples, each of which is a 28×28 pixel grayscale handwritten digital image and represents a number from 0 to 9.

4.2.1. Comparison of the multi-GENEO, multi-DGENEO, and mix-GENEO using binary classification

We will give examples of multi-GENEO, multi-DGENEO, and mix-GENEO persistence filtrations to validate the effectiveness of our multifiltrations on the MNIST dataset. We compare the performances of multi-GENEO, multi-DGENEO, and mix-GENEO filtrations for binary classification 0 and 1, 1 and 3, and 6 and 9. One can see that the mix-GENEO performs the best on the MNIST dataset in Table 1.

We plot the average persistence landscape for the digits $\{0, 1, 3, 6, 9\}$ (see Figures 7 and 8). Figures 7 and 8 show that though 1 has the same topological information as 3, as both have 1 connected component and no higher-dimensional cycles, the H_1 of digit 1 is significantly different from digits $s \in \{0, 3, 6, 9\}$ since they have different geometric information. It is worthy to note that although the topological and geometric information of 6 and 9 are almost the same, we still can find significant differences between them.

All landscapes of the numbers from 0 to 9 can be found in our github code.

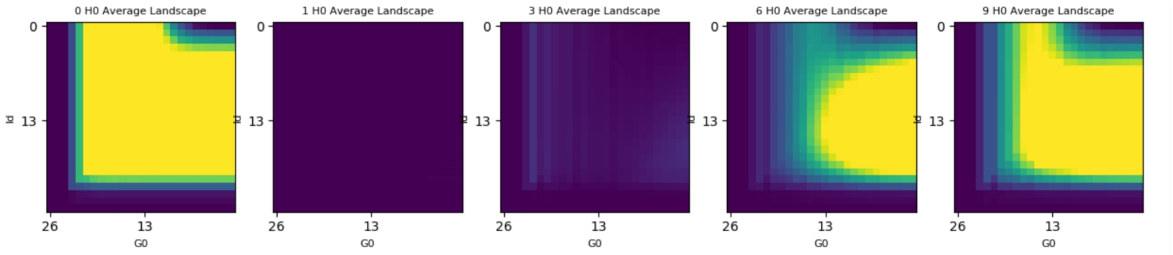

Figure 7. Multi-GENEO: Average multiparameter persistence landscape for each digit in $\{0, 1, 3, 6, 9\}$ in the MNIST dataset (H_0).

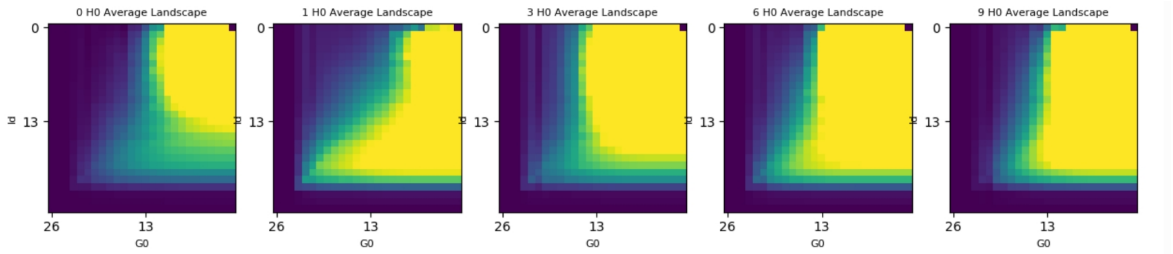

Figure 8. Multi-GENEO: Average multiparameter persistence landscape for each digit in $\{0, 1, 3, 6, 9\}$ in the MNIST dataset (H_1).

Results. We obtain the accuracies of binary classifications of 0 and 1, 1 and 3, and 6 and 9 by multiparameter persistence landscapes of the multi-GENEO, multi-DGENEO, and mix-GENEO, respectively. For the MNIST dataset, we use their train and test datasets for training and testing. More details of the results are provided in Table 1. The accuracy of the mix-GENEO of binary classification of 0 and 1, which have different topological information, can achieve 99.8%. The accuracy of the mix-GENEO of binary classification of 6 and 9, which have almost the same topological and geometric information, can achieve 95.1% for concatenated H_0 and H_1 features. The accuracy of mix-GENEO of binary classification of 1 and 3, which have different geometric information, can achieve 99.2%. In our

three methods, the mix-GENEO performs the best for H_0, H_1, and concatenated H_0 and H_1 features. The results demonstrate that our multiparameter filtration mix-GENEO more effectively characterizes topological and geometric features. Moreover, for multiparameter filtrations, both the GENEO and DGENEO are necessary.

Table 1. Binary classification results of multi-GENEO, multi-DGENEO, and mix-GENEO for the MNIST dataset using PCA+SVM, RF, and CNN. In the first row, the following abbreviation is used: PS=PCA+SVM. $H_0 + H_1$ is the concatenated H_0 and H_1 features. Bold indicates the highest scores.

		H_0			H_1			$H_0 + H_1$		
		PS	RF	CNN	PS	RF	CNN	PS	RF	CNN
0 vs 1	mul-G	98.8	99.0	99.1	63.9	62.7	63.9	98.7	99.2	99.3
	mul-D	60.2	60.4	60.2	87.5	95.5	88.6	87.8	95.2	89.3
	mix-G	**99.3**	**99.6**	**99.5**	**96.2**	**99.3**	**99.3**	**99.4**	**99.6**	**99.8**
1 vs 3	mul-G	72.3	73.0	73.2	67.6	68.3	68.0	70.3	79.9	80.1
	mul-D	59.4	59.4	60.0	73.6	75.2	75.5	66.5	76.3	77.2
	mix-G	**96.2**	**97.3**	**97.2**	**84.2**	**98.7**	**98.7**	**99.1**	**99.1**	**99.2**
6 vs 9	mul-G	68.6	69.0	70.3	52.4	55.9	54.2	79.0	69.0	71.3
	mul-D	54.3	51.5	52.3	**67.0**	66.2	67.3	75.2	68.1	64.5
	mix-G	**83.9**	**86.7**	**86.3**	66.6	**84.3**	**86.7**	**94.1**	**95.2**	**95.1**

4.2.2. Comparison of 1-parameter filtrations, the multi-GENEO, the multi-DGENEO, and the mix-GENEO using ten-classification

We also compare the performances of lower-star filtration, upper-star filtration, height filtration, radial filtration, density filtration, the multi-GENEO, the multi-DGENEO, and the mix-GENEO persistence filtrations for ten-classification.

Results. The accuracies of ten-classification are shown in Table 2. One can see that the mix-GENEO performs best. It can effectively identify ten classes and achieve an accuracy of 80.6%.

Table 2. Ten-classification results of the lower-star, upper-star, height, radial, density, multi-GENEO, multi-DGENEO, and mix-GENEO for the MNIST dataset using PCA+SVM, RF, and CNN. In the first row, the following abbreviation is used: PS=PCA+SVM. $H_0 + H_1$ is the concatenated H_0 and H_1 features. Bold indicates the highest scores.

	H_0			H_1			$H_0 + H_1$		
	PS	RF	CNN	PS	RF	CNN	PS	RF	CNN
lower-star	30.0	29.8	30.0	15.3	15.2	15.4	33.4	32.6	33.6
upper-star	14.5	14.4	14.6	30.0	29.8	30.1	32.5	31.8	32.8
height	34.3	34.3	34.3	27.7	27.7	27.8	55.0	55.0	55.0
radial	25.8	25.8	26.0	31.9	31.9	32.0	45.8	45.9	45.9
density	18.9	18.9	18.9	31.9	31.9	32.0	45.8	45.9	45.9
mul-G	39.7	41.0	42.1	19.3	19.0	19.7	43.4	44.0	45.8
mul-D	14.2	14.6	14.9	29.4	31.7	32.1	31.0	30.3	33.2
mix-G	**67.8**	**67.8**	**72.1**	**50.6**	**47.6**	**52.9**	**78.8**	**78.3**	**80.6**

5. Conclusions and future work

In this paper, we introduce three multiparameter persistence filtrations called the multi-GENEO, multi-DGENEO, and mix-GENEO, which can be chosen flexibly. Moreover, we show the stability of both the interleaving distance and multiparameter persistence landscape of the multi-GENEO persistence modules. We also provide estimations of the upper bound for multi-DGENEO and mix-GENEO persistence module with respect to pseudometrics. After giving an algorithm to build the bifiltrations on digital images, the experiments we conducted demonstrate that our methods perform better than 1-parameter filtrations, and that our methods can significantly distinguish not only the ones with different topological information but also the ones with almost the same topological and geometric information.

In future work, we would like to develop our methods in the following two aspects. On the one hand, we plan to optimize our methods to get better results. For instance, we would obtain multiparameter filtrations by higher dimensional sublevelset functions or by selecting suitable operators in another way. We would like to thank the reviewer for suggesting that we work with more complex datasets. In our future research, we will adopt optimization methods to develop operators suitable for more complex datasets (e.g. the CIFAR-10 dataset). On the other hand, we plan to apply our methods to other fields or problems, for instance, integrating features into deep learning and medical research.

Author contributions

Jiaxing He: Conceptualization, software, methodology, writing-original draft; Bingzhe Hou: Conceptualization, methodology, formal analysis, writing – review & editing; Tieru Wu: Supervision, writing – review & editing; Yue Xin: Methodology, validation, writing – review & editing. All authors have read and approved the final version of the manuscript for publication.

Use of Generative-AI tools declaration

The authors declare that they have not used Artificial Intelligence (AI) tools in the creation of this article.

Acknowledgments

The authors would like to thank the editor and the reviewers for their dedicated time and constructive comments. This work is supported by the National Key Research and Development Program of China (Grant No. 2022YFB3103702).

Code availability

Our code is available at `https://github.com/HeJiaxing-hjx/Mix-GENEO/`.

Conflict of interest

The authors declare that there are no conflicts of interest in this work.

References

1. H. Adams, M. Aminian, E. Farnell, M. Kirby, J. Mirth, R. Neville, et al., A fractal dimension for measures via persistent homology, In: *Topological data analysis*, Cham: Springer, 2020, 1–31. https://doi.org/10.1007/978-3-030-43408-3_1
2. H. Adams, T. Emerson, M. Kirby, R. Neville, C. Peterson, P. Shipman, et al., Persistence images: A stable vector representation of persistent homology, *J. Mach. Learn. Res.*, **18** (2017), 1–35.
3. H. Adams, M. Moy, Topology applied to machine learning: From global to local, *Front. Artif. Intell.*, **4** (2021), 668302. https://doi.org/10.3389/frai.2021.668302
4. H. Anai, F. Chazal, M. Glisse, Y. Ike, H. Inakoshi, R. Tinarrage, et al., DTM-based filtrations, In: *Topological data analysis*, Cham: Springer, 2020, 33–66. https://doi.org/10.1007/978-3-030-43408-3_2
5. U. Bauer, M. B. Botnan, S. Oppermann, J. Steen, Cotorsion torsion triples and the representation theory of filtered hierarchical clustering, *Adv. Math.*, **369** (2020), 107171. https://doi.org/10.1016/j.aim.2020.107171
6. M. G. Bergomi, P. Frosini, D. Giorgi, N. Quercioli, Towards a topological–geometrical theory of group equivariant non-expansive operators for data analysis and machine learning, *Nat. Mach. Intell.*, **1** (2019), 423–433. https://doi.org/10.1038/s42256-019-0087-3
7. B. Bleile, A. Garin, T. Heiss, K. Maggs, V. Robins, The persistent homology of dual digital image constructions, In: *Research in computational topology 2*, Cham: Springer, 2022, 1–26. https://doi.org/10.1007/978-3-030-95519-9_1

8. A. J. Blumberg, I. Gal, M. A. Mandell, M. Pancia, Robust statistics, hypothesis testing, and confidence intervals for persistent homology on metric measure spaces, *Found. Comput. Math.*, **14** (2014), 745–789. https://doi.org/10.1007/s10208-014-9201-4
9. A. J. Blumberg, M. Lesnick, Universality of the homotopy interleaving distance, *Trans. Amer. Math. Soc.*, **376** (2023), 8269–8307. https://doi.org/10.1090/tran/8738
10. A. J. Blumberg, M. Lesnick, Stability of 2-parameter persistent homology, *Found. Comput. Math.*, **24** (2024), 385–427. https://doi.org/10.1007/s10208-022-09576-6
11. O. Bobrowski, S. Mukherjee, J. E. Taylor, Topological consistency via kernel estimation, *Bernoulli*, **23** (2017), 288–328. https://doi.org/10.3150/15-BEJ744
12. M. B. Botnan, M. Lesnick, An introduction to multiparameter persistence, *arXiv preprint arXiv:2203.14289*, 2023. https://doi.org/10.48550/arXiv.2203.14289
13. R. Brüel-Gabrielsson, B. J. Nelson, A. Dwaraknath, P. Skraba, L. J. Guibas, G. Carlsson, A topology layer for machine learning, *arXiv:1905.12200*, 2020. http://arxiv.org/abs/1905.12200
14. P. Bubenik, Statistical topological data analysis using persistence landscapes, *J. Mach. Learn. Res.*, **16** (2015), 77–102.
15. P. Bubenik, M. Hull, D. Patel, B. Whittle, Persistent homology detects curvature, *Inverse Probl.*, **36** (2020), 025008. https://doi.org/10.1088/1361-6420/ab4ac0
16. M. Buchet, F. Chazal, S. Y. Oudot, D. R. Sheehy, Efficient and robust persistent homology for measures, *Comput. Geom.*, **58** (2016), 70–96. https://doi.org/10.1016/j.comgeo.2016.07.001
17. G. Carlsson, T. Ishkhanov, V. de Silva, A. Zomorodian, On the local behavior of spaces of natural images, *Int. J. Comput. Vis.*, **76** (2008), 1–12. https://doi.org/10.1007/s11263-007-0056-x
18. G. Carlsson, G. Singh, A. Zomorodian, Computing multidimensional persistence, In: *Algorithms and computation*, Berlin: Springer, **5878** (2009), 730–739. https://doi.org/10.1007/978-3-642-10631-6_74
19. G. Carlsson, A. Zomorodian, The theory of multidimensional persistence, *Discrete Comput. Geom.*, **42** (2009), 71–93. https://doi.org/10.1007/s00454-009-9176-0
20. M. Carrieère, A. Blumberg, Multiparameter persistence image for topological machine learning, In: *Advances in neural information processing systems*, 2020.
21. F. Chazal, L. J. Guibas, S. Y. Oudot, P. Skraba, Scalar field analysis over point cloud data, *Discrete Comput. Geom.*, **46** (2011), 743–775. https://doi.org/10.1007/s00454-011-9360-x
22. Y. M. Chung, S. Day, C. S. Hu, A multi-parameter persistence framework for mathematical morphology, *Sci. Rep.*, **12** (2022), 6427. https://doi.org/10.1038/s41598-022-09464-7
23. D. Cohen-Steiner, H. Edelsbrunner, D. Morozov, Vines and vineyards by updating persistence in linear time, In: *Proceedings of the twenty-second annual symposium on Computational geometry*, 2006, 119–126. https://doi.org/10.1145/1137856.1137877
24. F. Conti, D. Moroni, M. A. Pascali, A topological machine learning pipeline for classification, *Mathematics*, **10** (2022), 3086. https://doi.org/10.3390/math10173086
25. R. Corbet, M. Kerber, M. Lesnick, G. Osang, Computing the multicover bifiltration, *Discrete Comput. Geom.*, **70** (2023), 376–405. https://doi.org/10.1007/s00454-022-00476-8

26. W. Crawley-Boevey, Decomposition of pointwise finite-dimensional persistence modules, *J. Algebra Appl.*, **14** (2015), 1550066. https://doi.org/10.1142/S0219498815500668

27. H. Edelsbrunner, J. Harer, Persistent homology–A survey, *Contemp. Math.*, **453** (2008), 257–282.

28. H. Edelsbrunner, G. Osang, The multi-cover persistence of Euclidean balls, *Discrete Comput. Geom.*, **65** (2021), 1296–1313. https://doi.org/10.1007/s00454-021-00281-9

29. P. Frosini, *G*-invariant persistent homology, *Math. Method. Appl. Sci.*, **38** (2015), 1190–1199. https://doi.org/10.1002/mma.3139

30. P. Frosini, G. Jabłoński, Combining persistent homology and invariance groups for shape comparison, *Discrete Comput. Geom.*, **55** (2016), 373–409. https://doi.org/10.1007/s00454-016-9761-y

31. A. Garin, G. Tauzin, A topological "reading" lesson: Classification of mnist using tda, In: *2019 18th IEEE international conference on machine learning and applications (ICMLA)*, USA: IEEE, 2019, 1551–1556. https://doi.org/10.1109/ICMLA.2019.00256

32. L. Guibas, D. Morozov, Q. Mérigot, Witnessed *k*-distance, *Discrete Comput. Geom.*, **49** (2013), 22–45. https://doi.org/10.1007/s00454-012-9465-x

33. O. Hacquard, K. Balasubramanian, G. Blanchard, C. Levrard, W. Polonik, Topologically penalized regression on manifolds, *J. Mach. Learn. Res.*, **23** (2022), 1–39.

34. A. Hatcher, *Algebraic topology*, Cambridge: Cambridge University Press, 2001.

35. C. Hofer, R. Kwitt, M. Niethammer, M. Dixit, Connectivity-optimized representation learning via persistent homology, In: *Proceedings of the 36th international conference on machine learnin*, 2019.

36. C. Hofer, R. Kwitt, M. Niethammer, A. Uhl, Deep learning with topological signatures, In: *Advances in neural information processing systems*, 2017.

37. M. Lesnick, The theory of the interleaving distance on multidimensional persistence modules, *Found. Comput. Math.*, **15** (2015), 613–6505. https://doi.org/10.1007/s10208-015-9255-y

38. M. Lesnick, M. Wright, Interactive visualization of 2-d persistence modules, *arXiv:1512.00180*, 2015. https://doi.org/10.48550/arXiv.1512.00180

39. D. Loiseaux, M. Carrière, A. Blumberg, A framework for fast and stable representations of multiparameter persistent homology decompositions, In: *Advances in neural information processing systems*, **36** (2023).

40. E. R. Love, B. Filippenko, V. Maroulas, G. Carlsson, Topological convolutional layers for deep learning, *J. Mach. Learn. Res.*, **24** (2023), 1–35.

41. C. Maria, J. D. Boissonnat, M. Glisse, M. Yvinec, The gudhi library: Simplicial complexes and persistent homology, In: *Mathematical software–ICMS 2014*, Berlin: Springer, **8592** (2014). https://doi.org/10.1007/978-3-662-44199-2_28

42. D. Morozov, Dionysus 2. Available from: `https://mrzv.org/software/dionysus2/`.

43. S. Y. Oudot, Persistence theory: From quiver representations to data analysis, In: *Mathematical surveys and monographs*, American Mathematical Society, 2017.

44. J. M. Phillips, B. Wang, Y. Zheng, Geometric inference on kernel density estimates, *arXiv:1307.7760*, 2013. https://doi.org/10.48550/arXiv.1307.7760

45. L. Polterovich, D. Rosen, K. Samvelyan, J. Zhang, Topological persistence in geometry and analysis, In: *University lecture series*, American Mathematical Society, **74** (2020).

46. R. Rabadán, A. J. Blumberg, *Topological data analysis for genomics and evolution: Topology in biology*, Cambridge: Cambridge University Press, 2019.

47. V. Robins, P. J. Wood, A. P. Sheppard, Theory and algorithms for constructing discrete morse complexes from grayscale digital images, *IEEE Trans. Pattern Anal. Mach. Intell.*, **33** (2011), 1646–1658. https://doi.org/10.1109/TPAMI.2011.95

48. N. Saul, C. Tralie, *Scikit-TDA: Topological data analysis for python*, 2019. http://doi.org/10.5281/zenodo.2533369

49. B. Schweinhart, Fractal dimension and the persistent homology of random geometric complexes, *Adv. Math.*, **372** (2020), 107291.

50. B. Schweinhart, Persistent homology and the upper box dimension, *Discrete Comput. Geom.*, **65** (2021), 331–364. https://doi.org/10.1007/s00454-019-00145-3

51. Y. E. Solomon, P. Bendich, Convolutional persistence transforms, *J. Appl. Comput. Topology*, **8** (2024), 1981–2013. https://doi.org/10.1007/s41468-024-00164-x

52. The RIVET Developers, Rivet, 2020. Available from: `https://github.com/rivetTDA/rivet/`.

53. O. Vipond, Multiparameter persistence landscapes, *J. Mach. Learn. Res.*, **21** (2020), 1–38.

54. O. Vipond, J. A. Bull, P. S. Macklin, U. Tillmann, C. W. Pugh, H. M. Byrne, et al., Multiparameter persistent homology landscapes identify immune cell spatial patterns in tumors, *Proc. Natl. Acad. Sci. U.S.A.*, **118** (2021), e2102166118. https://doi.org/10.1073/pnas.2102166118

55. A. Zomorodian, G. Carlsson, Computing persistent homology, *Discrete Comput. Geom.*, **33** (2005), 249–274. https://doi.org/10.1007/s00454-004-1146-y

56. A. J. Zomorodian, Topology for computing, In: *Cambridge monographs on applied and computational mathematics*, Cambridge: Cambridge University Press, 2009. https://doi.org/10.1017/CBO9780511546945

A. Appendix

We present the GENEOs (G_0, G_1, G_2, G_3, G_4) and DGENEOs ($G_2 - G_1$, $G_4 - G_3$) used in our study in Figures 9 and 10, respectively.

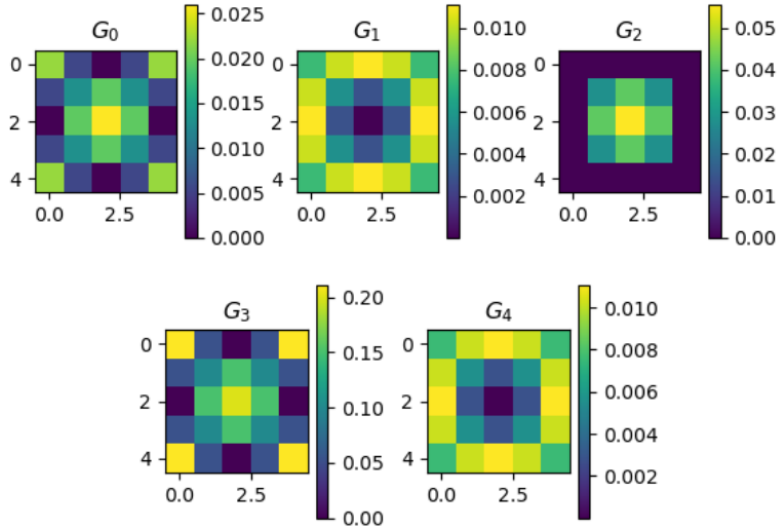

Figure 9. GENEOs.

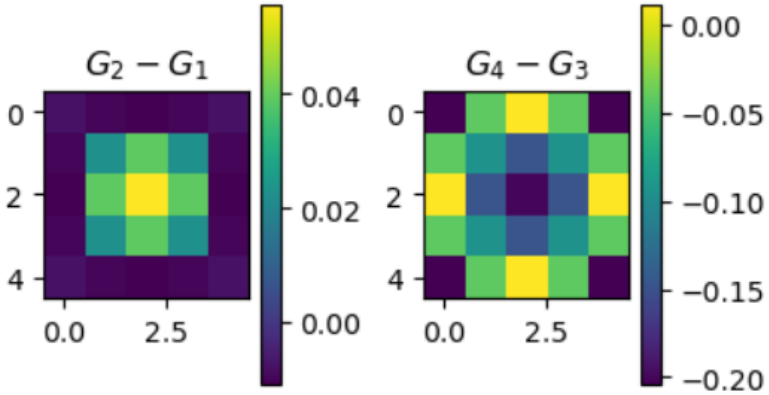

Figure 10. DGENEOs.

Recall that our multi-GENEO filtration is built by G_0 and Id acting on φ via right composition. Multi-DGENEO fitration is built by $\varphi \circ (G_4 - G_3)$ and $\varphi \circ (G_2 - G_1)$, and mix-GENEO filtration is built by $\varphi \circ G_0$ and $\varphi \circ (G_4 - G_3)$.

Taking the digit 5 in MNIST as an example, we show the $\varphi \circ \mathrm{Id}$, $\varphi \circ G_0$, $\varphi \circ (G_2 - G_1)$, and $\varphi \circ (G_4 - G_3)$ that we specifically used to build multi-GENEO, multi-DGENEO, and mix-GENEO filtrations in Figure 11 (φ here is the digit 5).

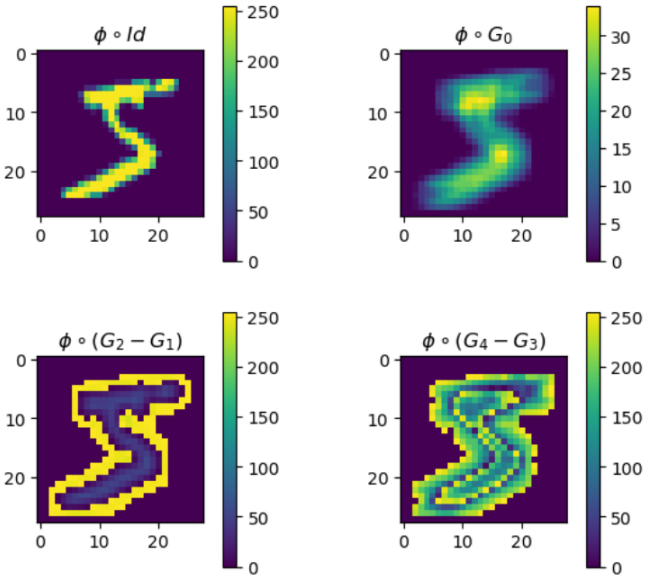

Figure 11. Examples of $\varphi \circ \mathrm{Id}$, $\varphi \circ G_0$, $\varphi \circ (G_2 - G_1)$, and $\varphi \circ (G_4 - G_3)$.